Journal of Colloid and Interface Science 609 (2022) 54–64

Contents lists available at ScienceDirect

Journal of Colloid and Interface Science

journal homepage: www.elsevier.com/locate/jcis

Synthesis of carbon dots with strong luminescence in both dispersed and aggregated states by tailoring sulfur doping

Xianjing Li [a,b,1], Mengdan Zheng [a,b,1], Haijing Wang [c], Yuan Meng [d], Duan Wang [a,b], Lili Liu [a,b], Qinghui Zeng [e], Xiaowei Xu [a,b,*], Ding Zhou [e,*], Hongchen Sun [a,b,*]

[a] Hospital of Stomatology, Jilin University, Changchun 130021, PR China
[b] Jilin Provincial Key Laboratory of Tooth Development and Bone Remodeling, Jilin University, Changchun 130021, PR China
[c] Department of Chemistry, Durham University, Durham DH1 3LE, UK
[d] School and Hospital of Stomatology, China Medical University, Shenyang 110122, PR China
[e] State Key Laboratory of Luminescence and Applications, Changchun Institute of Optics, Fine Mechanics and Physics, Chinese Academy of Sciences, Changchun 130033, PR China

GRAPHICAL ABSTRACT

Carbon dots (CDots) with a strong greenish-yellow fluorescence in both dispersed and aggregated states are prepared. The as-prepared CDots with a size of 3.5 nm possess excellent biocompatibility, good photostability, strong solid-state luminescence, and remarkable resistance to organic solvent, allowing their applications in biological imaging *in vitro* and *in vivo* and as the color conversion layer for white light-emitting diodes.

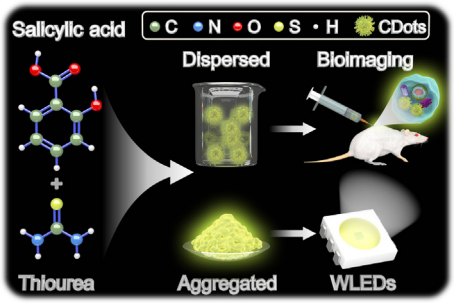

ARTICLE INFO

Article history:
Received 24 September 2021
Revised 17 November 2021
Accepted 28 November 2021
Available online 1 December 2021

Keywords:
Nanomaterial
Carbon dot
Solid-state luminescence
Bioimaging
Light-emitting diode

ABSTRACT

Carbon dots (CDots), a class of environmentally friendly carbon-based luminescent nanomaterial, have been applied in a wide variety of fields, including bioimaging and light-emitting diodes (LEDs). Prior to these applications, however, CDots usually require modifications because some of its limitations (*e.g.*, the aggregation-induced luminescence quenching) make it difficult to apply in solid state. In order to realize CDots-based multiple applications simultaneously, this paper examines how CDots with a strong greenish-yellow fluorescence in both dispersed and aggregated states are prepared by microwave-assisted heating salicylic acid and thiourea. Based on control testing and the analysis of density functional theory calculations, S element from thiourea is doped into CDots and proves to be critical in governing the photoluminescence (PL) emission color. Featured with excellent biocompatibility and photostability, the dispersed CDots with photoluminescence quantum yields (32%) are able to function as a biological imaging reagent *in vitro* and *in vivo* without any side effect. Furthermore, the aggregated CDots also exhibit high photoluminescence quantum yields (26%) and remarkable resistance to organic solvent. These

* Corresponding authors.
E-mail addresses: xiaoweixu@jlu.edu.cn (X. Xu), zhouding@ciomp.ac.cn (D. Zhou), hcsun@jlu.edu.cn (H. Sun).
[1] These authors contributed equally to this work

https://doi.org/10.1016/j.jcis.2021.11.179

advantages will ensure that S-doped CDots can be applied as a color conversion layer so that white LEDs with different Commission International de L'Eclariage coordinates and tunable color temperature can be fabricated.

1. Introduction

Luminescent materials have been applied in various fields, including sensing, medical diagnostics and therapy [1], bioimaging [2], light-emitting diodes (LEDs) [3], and so forth [4]. Especially, luminescent materials with a strong PL emission in both dispersed and aggregated states are in high demand. The luminescent materials presently available are mainly rare-earth-based materials, semiconductor quantum dots (QDs), perovskite QDs and organic dyes. Despite their achievements in promoting the revolution in optics, however, there are still several concerns and issues to be addressed. Rare-earth-doped nanoparticles are currently in severe shortage and non-renewable [5]. The high-performance QDs tend to bring the concerns of environmental destruction due to the involved toxic heavy metal elements [6], and organic dyes show weak stability. Consequently, the development of novel luminescent materials is essential for improving their performance, including safety, cost and stability and thereby extending the prospect of their applications.

Recently, carbon dots (CDots), as a class of emerging and environmentally friendly carbon-based luminescent nanomaterial [7–10], have received great scholarly interest owing to their distinct advantages [11–17], such as easy and eco-friendly preparation [18], low cost [19], low toxicity [20], long-term preservation [21], adjustable luminescence [22], high photoluminescence quantum yields (PLQYs) [23], and excellent resistance to photobleaching [24]. Based on these characteristics, CDots have ignited tremendous interest in photocatalysis, energy storage and conversion, biosensors, bioimaging, LEDs, and so forth [25–35]. In particular, the small particle size of CDots is conducive to enter the living body for bioimaging, and the *in vivo* administration of CDots has no significant side effects, which could be proved by the biological safety indicators [36–38]. Besides, the capability to control the PL emission properties of CDots allows us to fabricate white LEDs (WLEDs) with controllable color temperatures, where CDots are applied as a color conversion layer [39–41]. As can be seen from the above description, when applying CDots in these applications, CDots had better possess a strong PL emission in both dispersed and aggregated states [42]. Nevertheless, most of the CDots reported in previous studies are capable of exhibiting bright luminescence and high PLQYs in dispersed state (*i.e.*, in solution), whereas the aggregated CDots show nearly no PL emission and very low PLQYs due to the resonance energy transfer and direct π–π interactions (similar to the interactions in organic molecules) between CDots in the aggregate state (also known as the aggregation-induced luminescence quenching) [13,41,43–46]. As a result, CDots are requested to be treated by chemical/physical modifications before being used in multiple applications simultaneously.

To avoid the aggregation-induced luminescence quenching, several encapsulation methods have been proposed to disperse the CDots into matrix, including silica [47], trisodium citrate [48], zeolites [49], polyhedral oligomeric silsesquioxane, and so forth [50]. In doing so, their PL properties are preserved in the solid state. However, despite numerous achievements of these researches, these methods are generally time-consuming and complicated, and the raw materials (including CDots and matrix) cannot be fully utilized during the preparation, resulting in a high cost but a low yield. More importantly, the resultant CDots-based composites usually have very poor water solubility and large particle size, which would limit, or even forbid the application of CDots in life science. Therefore, it is of great scientific value to construct CDots without aggregation-induced luminescence quenching for the development and optimization of CDots-based multifunctional luminescent materials.

Doping other elements into CDots is always an efficient way to improve their performance and expand their applications [25,51,52], including N element for increasing the PLQYs [53], S element for enhancing photocatalytic reactivity [54], Mg element for regulating photosynthetic activity [55], Ce element for promoting wound healing [56], and so forth. Especially, S element is abundant in nature and environment-friendly, and can eliminate O-states and enhance *N*-states of the CDots, therewith resulting in stronger PL emissions [57]. As a result, these accomplishments inspire us to develop the S doping strategy to address the aforementioned challenges (*i.e.*, aggregation-induced luminescence quenching). In this work, S-doped CDots with a strong greenish-yellow fluorescence in both dispersed and aggregated states are synthesized by heating salicylic acid and thiourea in a one-step microwave treatment, where the S element from thiourea plays a key role in controlling the PL properties of the CDots according to the control test and results of the theoretical calculations. The resultant CDots with a size of 3.5 nm possess a high PLQYs (32%) in the dispersed state, excellent biocompatibility, and good photostability, and thus can be applied as a biological imaging reagent *in vitro* and *in vivo* without side effects. Furthermore, the aggregated CDots also exhibit a high PLQYs (26%) in the solid state and remarkable resistance to organic solvent. Benefiting from these unique properties, WLEDs with CDots as the color conversion layer can have different Commission International de L'Eclariage (CIE) coordinates and tunable color temperature from 3735 to 6646 K (Fig. 1).

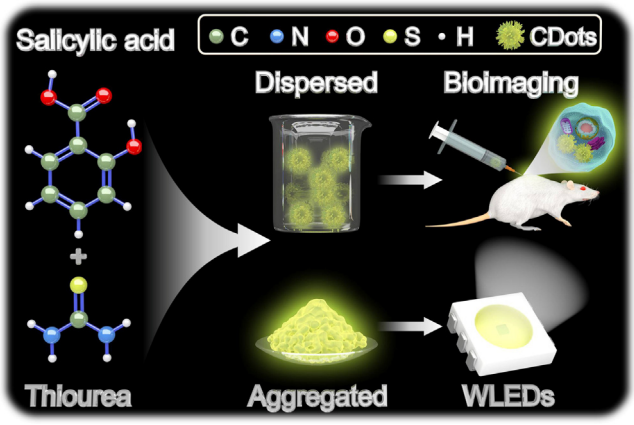

Fig. 1. Schematic illustration of the preparation of CDots with strong luminescence in both dispersed and aggregated states and their application in bioimaging and WLEDs.

2. Materials and methods

2.1. Materials

Salicylic acid (≥99.5%) and thiourea (99%) were purchased from Macklin Biochemical Co., Ltd (Shanghai, China). Epoxy-silicone resin A and B (98%), which were obtained from Ausbond, were used for encapsulation. Dulbecco's Modified Eagle Medium (DMEM) with high glucose, fetal bovine serum (FBS), and penicillin-streptomycin were obtained from Gibco (Grand Island, NY, USA), Biological Industries (Cromwell, CT, USA), and Hyclone (Logan, UT, USA), respectively. Phosphate buffered saline (PBS), dimethyl sulfoxide (DMSO) and 3-(4,5-dimethyl-2-thiazolyl)-2,5-diphenyl-2-H-tetrazolium bromide (MTT) were obtained from Amresco (Shanghai, China). Annexin Ⅴ-FITC/7-AAD apoptosis analysis kit was purchased from Tianjin Sungene Biotech Co., Ltd (Tianjin, China). Syringe filters with a pore size of 0.8 μm were purchased from Tianjin Jinteng Experimental Equipment Co., Ltd (Tianjin, China). Dialysis bag (MWCO = 1000 D) was purchased from Spectrum Laboratories (Rancho Dominguez, CA, USA). Ethanol was commercially available reagents. And in all experiments, the water was purified by distillation for twice.

2.2. Synthesis of carbon dots (CDots)

The S-doped CDots were synthesized by a one-step microwave treatment through condensation and further carbonization of salicylic acid and thiourea. In detail, 1.53 g of salicylic acid and 2.4 g of thiourea were added into 20 mL of deionized water, then the mixture was heated together in a household 500 W microwave oven, and the heating time is set to be 4 min for the complete carbonization. During this heating process, the system turned to brown liquid from the original colorless liquid, and finally formed a bright yellow clustered solid with strong greenish-yellow photoluminescence (*i.e.*, CDots). To get rid of small molecules, including some limited nanoscale carbon domains, molecular chromophores, organic dye-like species and so on, the as-prepared CDots were dialyzed in deionized water using a membrane with MWCO of 1000 D for one day. Next, anhydrous ethanol, deionized water and DMEM were utilized to dissolve the purified CDots at different concentrations for further use. Furthermore, the CDots powders (*i.e.*, the CDots aggregates) are obtained by freeze-drying the CDots solution. Following a similar procedure, except replacing thiourea with urea, CDots without S element were prepared for a comparison.

2.3. Characterizations of CDots

Photoluminescence (PL) data were obtained using a Shimadzu RF-5301 PC spectrophotometer. The excitation wavelength was adjustable. Ultraviolet–visible (UV–vis) absorption spectra were acquired utilizing a Lambda 800 UV–vis spectrophotometer. An Olympus BX-51 fluorescence microscope with a charge coupled device (CCD) camera was used to examine the photoluminescent materials. Transmission electron microscopy (TEM) and high-resolution TEM (HRTEM) images were conducted using a JEOL JEM-2100F TEM with a resolution of 0.1 nm at 200 kV. X-ray powder diffraction (XRD) test was carried out with Siemens D5005 diffractometer. Energy-dispersive spectroscopy (EDS) was measured by an Inca X-Max instrument. Fourier transform infrared (FTIR) spectra were obtained using a Nicolet AVATAR 360 FTIR instrument. Under the excitation of MG KR (1253.6 eV), the X-ray photoelectron spectroscopy (XPS) was performed *via* a VG ESCALAB MKII spectrometer. Binding energy calibration was based on C 1 s at 284.6 eV.

2.4. Computational methods

The ground states of two model CDots were all obtained from theoretical calculations by using density functional theory method as carried out in the Gaussian09 software package. The 6-31G* basis set was selected to combine with the functional B3LYP throughout all calculations (B3LYP/6-31G*). The green and red colors in the HOMO and LUMO molecular orbitals represent the positive and negative phases of the molecular orbital wavefunctions.

2.5. Toxicity assay of CDots in vitro

RAW264.7 cell line was derived from mouse monocyte macrophage cell (Chinese Academy of Sciences Cell Bank, Shanghai, China) and cultured in DMEM with high glucose, supplemented with 10% FBS and 1% penicillin/streptomycin. The cells were incubated in 5% CO_2 at 37 °C.

The cytotoxicity of the CDots was evaluated by MTT assay and cell apoptosis assay. MTT assay was performed in 96-well plates. RAW264.7 cells were seeded at 1×10^4 cells per well and cultured overnight. Then, the media were discarded and CDots were added to each well at a final concentration of 0, 10, 20, 50, 100 or 200 μg/mL. After another 24 h incubation, the media were removed and the wells were washed twice with PBS, and then100 μL of fresh culture medium with 20 μL of 5 mg/mL MTT was added to each well. After incubation for 4 h, the formazan crystals were observed at the bottom of the wells and the supernatants were removed. The crystals were dissolved in 150 μL of DMSO, and the absorbance was measured at 490 nm using a microplate reader (RT-6000; Lei Du Life Science and Technology Co, Shenzhen, China). The measurements were repeated three times, and the standard deviation was plotted as the error bar.

For cell apoptosis assay, RAW264.7 cells were seeded at 1×10^5 cells per well in a 6-well plate and cultured overnight. Then, the media were removed, and CDots were added to each well at a final concentration of 0, 10, 20, 50, 100 or 200 μg/mL. After 24 h incubation, the cells were harvested and stained according to the manufacturer's instructions of annexin V-FITC/7-AAD apoptosis analysis kit. Finally, the samples were analyzed by fluorescence-activated cell sorting (BD Biosciences, San Jose, CA, USA).

2.6. In vivo and in vitro fluorescence imaging

RAW264.7 cells were seeded at 1.5×10^5 cells/well in a 35 mm confocal dish and cultured overnight. Then the medium was removed, and the CDots were added to the well at a final concentration of 100 μg/mL. After 24 h incubation, the cells were washed three times with PBS and fixed in 95% ethanol for 30 min at 37 °C. Finally, the cells were washed twice with PBS, and then observed by confocal laser scanning microscopy (CLSM, Olympus, Japan) at 405 nm excitation.

The *in vivo* bioimaging of the CDots was performed in nude mice. All applicable institutional and/or national guidelines for the care and use of animals were followed. All animal procedures were performed in accordance with the Guidelines for Care and Use of Laboratory Animals of Jilin University and approved by the Animal Ethics Committee of No. 1 Hospital of Jilin University (approval number: 20200470). Six male nude mice (6-week old) were randomly divided into control group and CDots group. For the control group, 200 μL of PBS was injected subcutaneously at the middle of the back, whereas for the experimental group, 200 μL of CDots solution was injected at the same anatomical site. Then, the *in vivo* bioimaging photographs of the mice were taken by a CCD camera with a 450 nm filter (long pass) under UV light.

2.7. Toxicity assay of CDots in vivo

The *in vivo* toxicity of the CDots was evaluated after *in vivo* bioimaging mentioned above. The mice were euthanized and important organs, including hearts, livers and kidneys, were collected and fixed, dehydrated, embedded in paraffin, and stained with hematoxylin and eosin (H&E) staining.

2.8. Fabrication of luminescent bulks and light-emitting diodes (LEDs) from CDots

At first, the solid-state CDots powders were mixed with epoxy-silicone A and B, where the mass ratio of epoxy-silicone A and B is fixed to be 2:1. The mixture was then stirred for 1 min until the CDots show a uniform dispersion. Next, a vacuum oven was used to remove the air from the mixture. Afterwards, the mixture was poured into molds and baked for 1 h at 80 ° C, and then the fluorescent bulk materials were obtained.

The indium gallium nitride (InGaN) LED chips without packaging materials were purchased commercially, where the InGaN microchips were placed at the bottom of the LEDs base, and these LEDs could emit bright blue light (405 nm) as the working voltage is 3.0 V. For the color conversion layer, CDots without aggregation-induced luminescence quenching were mixed with epoxy-silicone resin A and B components. Especially, because of the high PLQYs of CDots, only 20 mg CDots powders are required for the white LEDs with CIE coordinates of (0.31, 0.33). Then, the mixtures as packaging materials were deposited on the InGaN LED chips. After curing at 80 ° C for 1 h, CDots-based white LEDs with different color temperatures were obtained.

3. Results and discussion

As described in the experimental section, the CDots were synthesized from condensation and carbonization of salicylic acid and thiourea by a one-step microwave treatment, and the heating time is set to be 4 min for the complete carbonization, during which the colorless aqueous solution turned into bright yellow solid with strong photoluminescence (*i.e.*, CDots) (Fig. 1). To get rid of small molecules, including some limited nanoscale carbon domains, molecular chromophores, organic dye-like species and so on, the as-prepared CDots were dialyzed in deionized water using a membrane with MWCO of 1000 D for one day. The purified CDots powders (*i.e.*, the CDots aggregates) are obtained by freeze-drying the CDots solution and presents bright yellow color under sunlight (Fig. 2b). In contrast, microwave-assisted heating salicylic acid or thiourea alone only resulted in white products with nearly no photoluminescence (Fig. S1). Correspondingly, as shown in the ultraviolet–visible (UV–vis) absorption spectra (Fig. S2), salicylic acid in ethanol gives rise to two absorption peaks at 235 and 303 nm, and thiourea in ethanol shows a peak at 242 nm and an absorbance shoulder at 265 nm, respectively. However, the CDots ethanol solution gives a different UV–vis absorption spectrum, where two absorption peaks locate at 250 and 320 nm (Fig. 2a). The differences between the photoluminescence and the UV–vis absorption spectra of the raw materials and CDots indicate the formation of CDots is due to the reaction between salicylic acid and thiourea.

To reveal the morphology and structure of the CDots, high-resolution transmission electron microscopy (HRTEM) and X-ray powder diffraction (XRD) are carried out. In Fig. 3a, the HRTEM image shows that CDots are well dispersed with an average diameter of 3.5 nm, which is also proved by the corresponding size distribution histogram (Fig. S3). The nanometer scale sizes of CDots can facilitate the entry of CDots into cells, and therefore benefit the bioimaging of CDots *in vitro*. The well-resolved lattice spacing of CDots can be observed to be 0.33 nm, which is consistent with the (002) crystallographic facets of graphitic carbon reported in previous research [58]. XRD pattern of CDots exhibits a significant single peak centered at 3.3 Å (Fig. 3b), which agrees well with the lattice parameters shown in the HRTEM image. Using an energy dispersive spectrum (EDS) investigation, the as-prepared CDots are proved to be composed of C, N, O and S elements. Among these elements, all of O and a portion of C belong to salicylic acid, while all of N and S, and the rest of C are from thiourea (Fig. 3c).

In order to reveal the chemical structure and the formation mechanism of CDots, Fourier transform infrared (FTIR) characterization is performed. The FTIR spectrum of salicylic acid exhibits a carboxylic C═O stretching vibration at 1670 cm^{-1}, a carboxylic C—O stretching vibration at 1292 cm^{-1}, and a carboxylic O—H bending vibration at 1325 cm^{-1} (Fig. 3d). All above-mentioned peaks are assigned to the carboxyl group. Additionally, a phenolic C—O stretching vibration at 1246 cm^{-1} and a phenolic O—H bending vibration at 1325 cm^{-1} are ascribed to the phenolic hydroxyl group (Fig. 3d). The broad band of O—H stretching vibrations ranging from 2900 to 3500 cm^{-1} is originated from both the carboxyl and phenolic hydroxyl groups. The FTIR spectrum of thiourea presents N—H stretching vibrations at 3100–3500 cm^{-1}, an N—H bending vibration at 1610 cm^{-1}, a C—N stretching vibration at 1080 cm^{-1}, and two *N*-C═S stretching vibrations at 1410 and 1475 cm^{-1}, indicating the presence of amine groups. The carboxyl/hydroxyl groups of salicylic acid and the amine groups of thiourea ensure the subsequent dehydration condensation and carbonization to form the CDots. The FTIR spectrum of CDots shows O—H/N—H stretching vibrations at 3000–3500 cm^{-1}, suggesting the existence of the hydroxyl and amine groups in CDots. Compared with the C═O stretching vibration of salicylic acid, the C═O stretching vibration of CDots shifts to 1620 cm^{-1}, which is consistent with the position of the amide I band. The N—H bending vibration of CDots shifted as well from 1610 cm^{-1} to 1540 cm^{-1} in comparison with thiourea, which consists with the position of the amide Ⅱ band. Besides, an absorption peak appears at 1390 cm^{-1}, which could be attributed to the C═S stretching vibration (Fig. 3d). These results reveal that the formation of CDots is based on dehydration condensation and further carbonization between the carboxyl/hydroxyl and amine groups (Fig. 3c).

XPS analysis is used to further confirm the structure and the formation mechanism of CDots (Fig. 3). As shown in Fig. 3e, the C 1 s spectrum of the as-prepared CDots shows four peaks located at 284.5, 285.1, 287.8 and 288.5 eV that are assigned to sp^2 C, sp^3 C, –CON- and –COO-, respectively. The strong sp^2 C peak at 284.5 eV suggests that CDots contain large conjugated sp^2-domains. In addition, it has been concluded that the lattice spacing of CDots (0.33 nm) in HRTEM image is very close to the interlayer spacing of graphite (Fig. 3a). Thus, these results demonstrate that CDots are mainly constituted of several graphene-like sheets, which is consistent with the previous reports [58]. Furthermore, the peak of –CON- at 287.8 eV proves the amidation reaction between salicylic acid and thiourea, and the peak of –COO- at 288.5 eV confirms the existence of the carboxyl groups, which agrees with the FTIR analysis (Fig. 3d). The O 1 s spectrum of CDots shows two peaks at 531.9 and 532.9 eV (Fig. 3g) that are attributed to –CON- and –COO-/–NO_3-, respectively. The peaks of –CON- and –COO- further verify the occurrence of the amidation process and the existence of the carboxyl groups, which is well consistent with the C 1 s spectrum. The N 1 s spectrum of CDots is fitted with three peaks centered at 399.7, 400.3, and 401.9 eV (Fig. 3f), which are assigned to –NH-, N-$(C)_3$, and –CON-, respectively, indicating the presence of the amine groups and the dehydration condensation. The S 2p spectrum of CDots shows two peaks at 161.9 and 163.2 eV (Fig. 3h), which are attributed to S $2p_{1/2}$ and S $2p_{3/2}$,

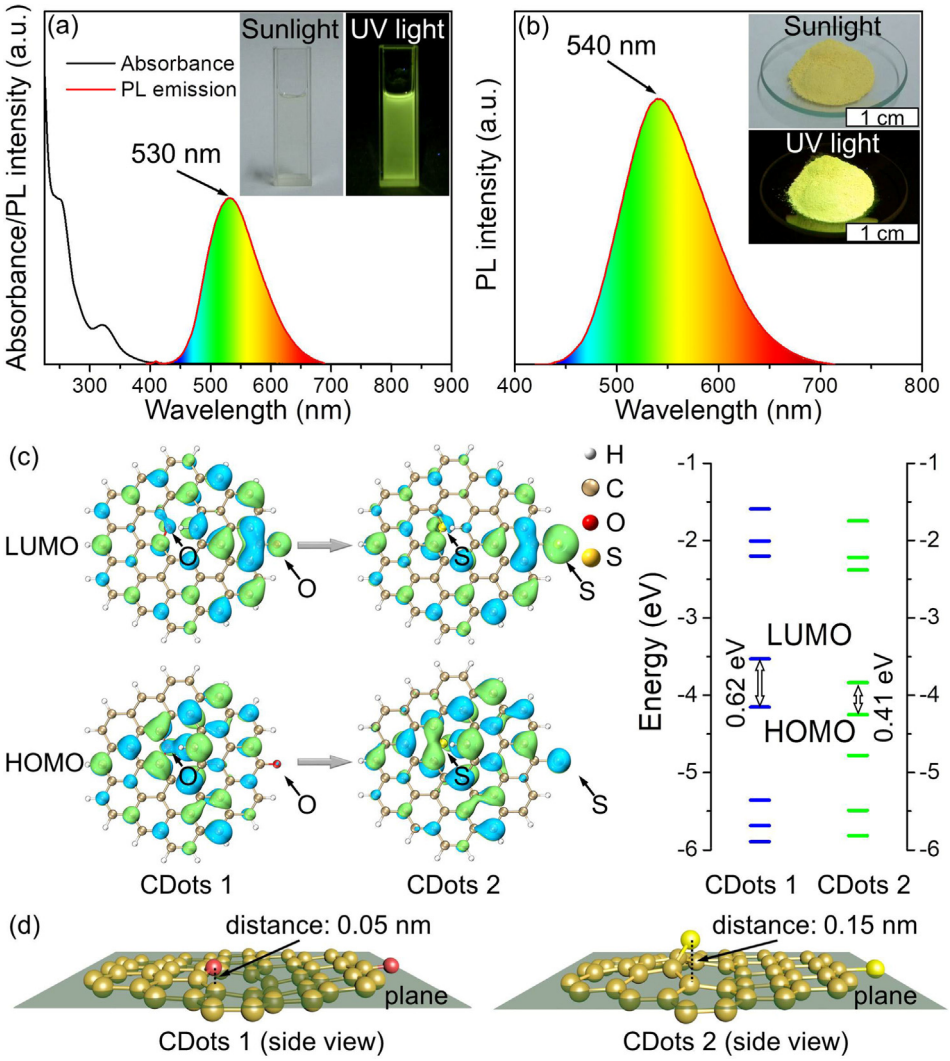

Fig. 2. The optical characterizations and density functional theory calculations of the CDots. (a) UV–vis absorption (black line) and PL emission (red line) spectra of the CDots solution. Insets: corresponding photographs taken under sunlight and UV light, respectively. (b) PL emission spectrum of the aggregated CDots. Insets: corresponding photographs taken under sunlight and UV light, respectively. (c) The DFT calculations of the electronic structure of CDots 1 and CDots 2 with corresponding orbital distribution of LUMO (the lowest unoccupied molecular orbital) and HOMO (the highest occupied molecular orbital). The isovalue is 0.02. The corresponding energy levels of CDots 1 and CDots 2. Here, CDots 1 and CDots 2 are the models of the CDots synthesized by salicylic acid/urea and salicylic acid/thiourea, respectively. (d) Side view of the optimized structures of CDots 1 and CDots 2, where the hydrogen atoms are not shown for clarity.

respectively, suggesting that S element is doped into CDots. In all, the XPS analysis, together with the FTIR and EDS characterizations, further demonstrates that the formation of CDots is conducted by the dehydration condensation and carbonization processes, during which CDots are doped with S element.

Furthermore, the CDots solution shows a bright greenish-yellow PL emission (the insets of Fig. 2a), and its PL emission spectra at different excitation wavelengths are shown in Fig. S4a. These spectra show that the PL emission peak locates at 530 nm under the best excitation wavelength of 405 nm, and the PLQYs of CDots is measured to be 32%, which is beneficial to the application of CDots in *in vitro* and *in vivo* bioimaging since naked eyes and detectors are highly sensitive to green light. Moreover, the greenish-yellow PL emission also allows CDots to be applied as the color conversion layer in fabricating WLEDs, because white light could be made up of blue and greenish-yellow light. Here, the existence of the doped S element in CDots plays a key role in determining the greenish-yellow PL emission of CDots. To verify this hypothesis, another CDots without the doped S element are synthesized through the same microwave-assisted heating method except using urea instead of thiourea (Fig. S6), where the chemical structure of urea and thiourea are the same except that the S element in thiourea is replaced by the O element in urea. And the resultant CDots prepared by urea and salicylic acid present a similar size and structure, but absence of S element (Fig. S5). The CDots solution without S element show a blue PL emission instead, centered at 475 nm with a low PLQYs of only 6% (Fig. S6a), whereas the CDots with doped S element (*i.e.*, synthesized by salicylic acid and thiourea) exhibit a bright greenish-yellow PL emission with a high PLQYs of 32%, indicating that the doping of S element could decrease the bandgap energy and improve the PL intensity. This conclusion is further confirmed by first-principles calculations based on density functional theory (DFT) using the B3LYP (Becke, 3-parameter, Lee-Yang-Parr) hybrid functional with the 6-31G* basis set (Table S1and S2).

According to the HRTEM and XPS analysis (Fig. 3a and 3e-h), the proposed simplified model is a monolayer graphene plate consisting of aromatic rings along with several heteroatoms, in which the only difference between these two models is that some O atoms in the first structure (CDots 1) are replaced *in situ* by S atoms in the

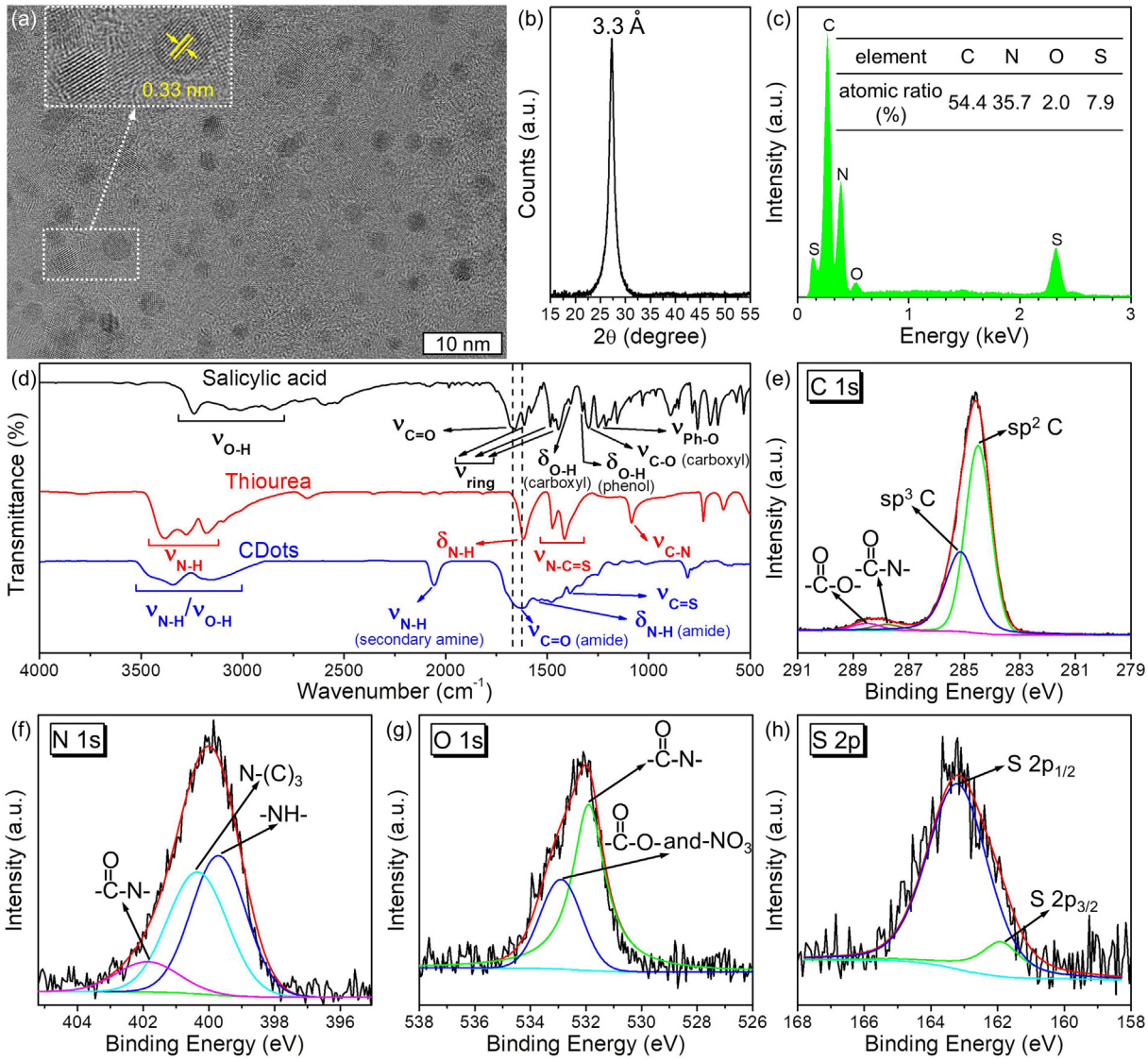

Fig. 3. The structural characterizations of the CDots. (a) HRTEM image of the CDots labeled by the yellow dotted line circle. (b) XRD pattern and (c) EDS spectrum of the CDots. The inset of (c) is a table showing the atomic ratios of the elements in CDots. (d) FTIR spectra of salicylic acid (black line), thiourea (red line) and CDots (blue line). (e-h) High-resolution XPS spectra of CDots: (e) C 1 s, (f) N 1 s, (g) O 1 s and (h) S 2p, respectively.

second structure (CDots 2) (Fig. 2c). After structure relaxation, the calculated bandgap energies decrease from 0.62 to 0.41 eV after doping with S element (Fig. 2c) [59]. This result further certifies the significant effect of the doped S element on achieving the greenish-yellow PL emission. More meaningfully, by freeze-drying the CDots solution, the CDots powders (*i.e.*, the CDots aggregates) are obtained and the as-prepared CDots also show a strong PL emission centered at 540 nm with a PLQY of 26% under the best excitation wavelength of 405 nm in the solid state (Fig. 2b and S4b). On the contrary, the aggregated CDots without S element possess a weak blue PL emission, centered at 481 nm with a low PLQYs of only 0.8% (Fig. S6b). So, the strong solid-state PL emission of CDots is originated from the effects of the doped S element on the structure. Based on the theoretical calculations, the best fit plane, which represents the sum of distances from each atom in the structure to this plane is minimal, is first obtained in both CDots 1 and CDots 2, and the distance from O or S atoms to the best fit planes are measured to be 0.05 and 0.15 nm, respectively (Fig. 2d). The larger distance from S atom to the plane can be understood in terms of the larger steric hindrance brought by S atom, whereas the size of O atom is very close to that of C atom. From a microscopic perspective, therefore, the structure of the CDots 2 is no more plane. Hence, intramolecular motion or π–π stacking is deteriorated in the aggregated state, leading to the solid-state PL emission of CDots synthesized by salicylic acid and thiourea and no aggregation-induced luminescence quenching [44,45]. In comparison with that of the CDots solution, the PL emission of the CDots powders shows a little red-shift of 10 nm at the same excitation wavelength, which is attributed to the PL emission reabsorption among the adjacent CDots. Besides, the dipole moment of CDots 2 is calculated to be 11.4 Debye, which is larger than that of CDots 1 (10.6 Debye), suggesting that the existence of S could increase the dipole moment. On the other hand, the rate of transition radiation is proportional to the dipole moment based on Fermi's golden rule [60]. Accordingly, doping S element is beneficial to enhance the PL intensity of CDots (*i.e.*, higher PLQYs). Furthermore, the effects of the S doping concentration on the PL properties are investigated (Fig. S7), and the results show that the optimal weight ratio of salicylic acid to thiourea is 1:1.5 for obtaining the CDots with a strong greenish-yellow PL emission.

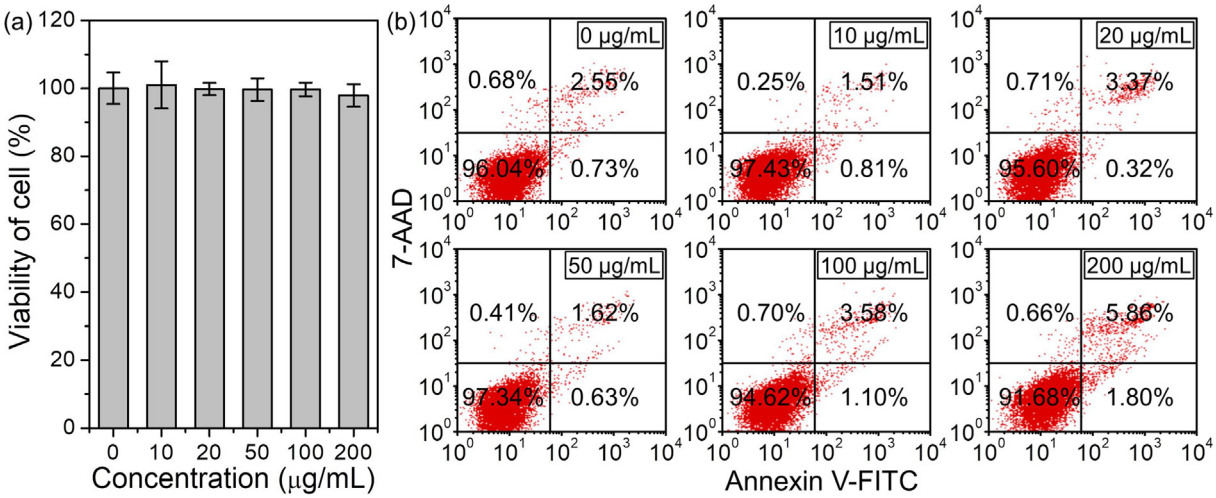

Fig. 4. Cytotoxicity assays of CDots. (a) MTT assay and (b) FACS data of apoptosis assay obtained from RAW264.7 cells, which are treated with different concentrations of CDots (10, 20, 50, 100, and 200 μg mL^{-1}). The measurements were repeated three times, and the standard deviation was plotted as error bar.

All these results indicate that the PL properties of the as-prepared CDots are greatly governed by the doped S element, and allow to be applied in bioimaging and color conversion layer for WLEDs simultaneously.

Since an important concern for applying materials in various practical applications is their good biosafety, Before *in vivo* and *in vitro* studies are carried out, we first evaluate the biocompatibility of CDots using 3-(4,5-dimethyl-2-thiazolyl)-2,5-diphenyl-2-H-tetrazolium bromide (MTT) assay and apoptosis assay. According to the result of MTT assay, there is no significant decrease in viabilities of RAW264.7 cells as the dosage of CDots increases from 0 to 200 μg/mL (Fig. 4a), demonstrating that CDots exhibit good biocompatibility and great potential in biological systems therewith. Furthermore, fluorescence-activated cell sorting (FACS) is conducted to reveal the effects of CDots on the apoptosis of RAW264.7 cells (Fig. 4b). Considering CDots possess a strong greenish-yellow fluorescence, annexin V-FITC/7-AAD apoptosis analysis kit is adopted in FACS assay, because the excitation/emission wavelength of FITC and 7-AAD are 498/515 nm and 550/645 nm, respectively, which would not be affected by the fluorescence of our CDots. From apoptosis assay, as the dosage of CDots increases from 0 to 200 μg/mL, the viabilities of RAW264.7 cells don't significantly decrease either. Both MTT and apoptosis assays have demonstrated that CDots have excellent biocompatibility and great potential in biological systems therewith, and can provide a basis for further *in vitro* and *in vivo* applications.

The stability of CDots is another concern for their further application. First, the photostability of CDots is investigated by using a common commercial fluorescent dye (*i.e.*, fluorescein sodium) as a comparison. The fluorescein sodium is a representative of the fluorescein-based bioimaging reagents, and it presents a green PL emission (Fig. S8). Then, the fluorescein sodium and CDots are continuously irradiated by a UV light (1.6 W cm^{-2}) under the same conditions, and their time-related PL intensities are recorded (Fig. S9). As seen from Fig. S9, the fluorescein sodium losses more than 30% of its initial PL intensity after the first 10 min of irradiation, and its PL decreases to 15% after 65 min of irradiation. In contrast, the PL intensity of CDots is still preserved more than 90% even after 65 min of irradiation. This suggests that CDots have excellent photostability to ensure its PL stability under the irradiation of the arc lamp/laser of fluorescence microscope.

Besides the good photostability, the as-prepared CDots exhibit remarkable resistance to common organic solvents as well, ensuring their PL stability when mixing them with the commericial packing materials containing organic solvents. To prove this, CDots are immersed in chloroform, and then the PL spectra and PLQYs of CDots powders before and after treatment are compared. As shown in Fig. S10a and b, CDots powders cannot be dissolved or swollen by chloroform. Under UV light, the supernatant chloroform solution has no photoluminescence, while the sediments(CDots powders) can preserve the strong greenish-yellow luminescence. The PL spectra of CDots powders before and after immersing into chloroform are nearly identical by normalizing the PL intensity, and both of their PLQYs are also measured to be the same one (*i.e.*, 32%) (Fig. S10c), indicating a high resistance of the CDots to organic solvents. This excellent solvent resistance allows the CDots to be directly mixed with commercial packing materials without the deterioration of the PL properties when processed toward LEDs. In order to confirm this proposal, the greenish-yellow fluorescent CDots powders without any treatment (*e.g.*, encapsulation by other matrixes) are straightly mixed with epoxy-silicone resin A and B (a common packing material), after which the mixture can be easily processed into different shapes of luminescent bulk materials by solidifying the mixture in different molds at 80 °C for 1 h (Fig. S10c). The bulk materials exhibit invariable greenish-yellow luminescence that is well consistent with the original CDots (Fig. S10c and d), suggesting that the CDots are not affected by the packing materials even if there are no additional matrixes to protect CDots. The uniform emissions of the entire bulk materials indicate that the CDots can be well distributed in the packaging bulk, which is mainly due to the powdered state of CDots. Therefore, all of the aforementioned advantages, including high PLQYs, small particle sizes, strong solid-state fluorescence, excellent biocompatibility, good photostability, as well as remarkable resistance to organic solvent, ensure the further applications of CDots in *in vitro* and *in vivo* bioimaging and LEDs.

In vitro fluorescence cell imaging is performed by incubating mouse leukemic monocyte macrophage RAW264.7 cells with CDots for 24 h. As shown in Fig. 5a-c, the confocal laser scanning microscopy (CLSM) images show that RAW264.7 cells treated by CDots possess bright luminescence under the excitation of 405 nm, revealing that the CDots can be internalized into the cells because of their nanosized diameter (Fig. 3a). In addition, as a result of the CDots' non-toxicity (Fig. 4), there are no variations in the morphology of the RAW264.7 cell after the treatment by CDots, demonstrating that the CDots have no effects on cell growth and development. This is of great significance to a cell imaging reagent, since it allows to examine the cellular evolution, but does

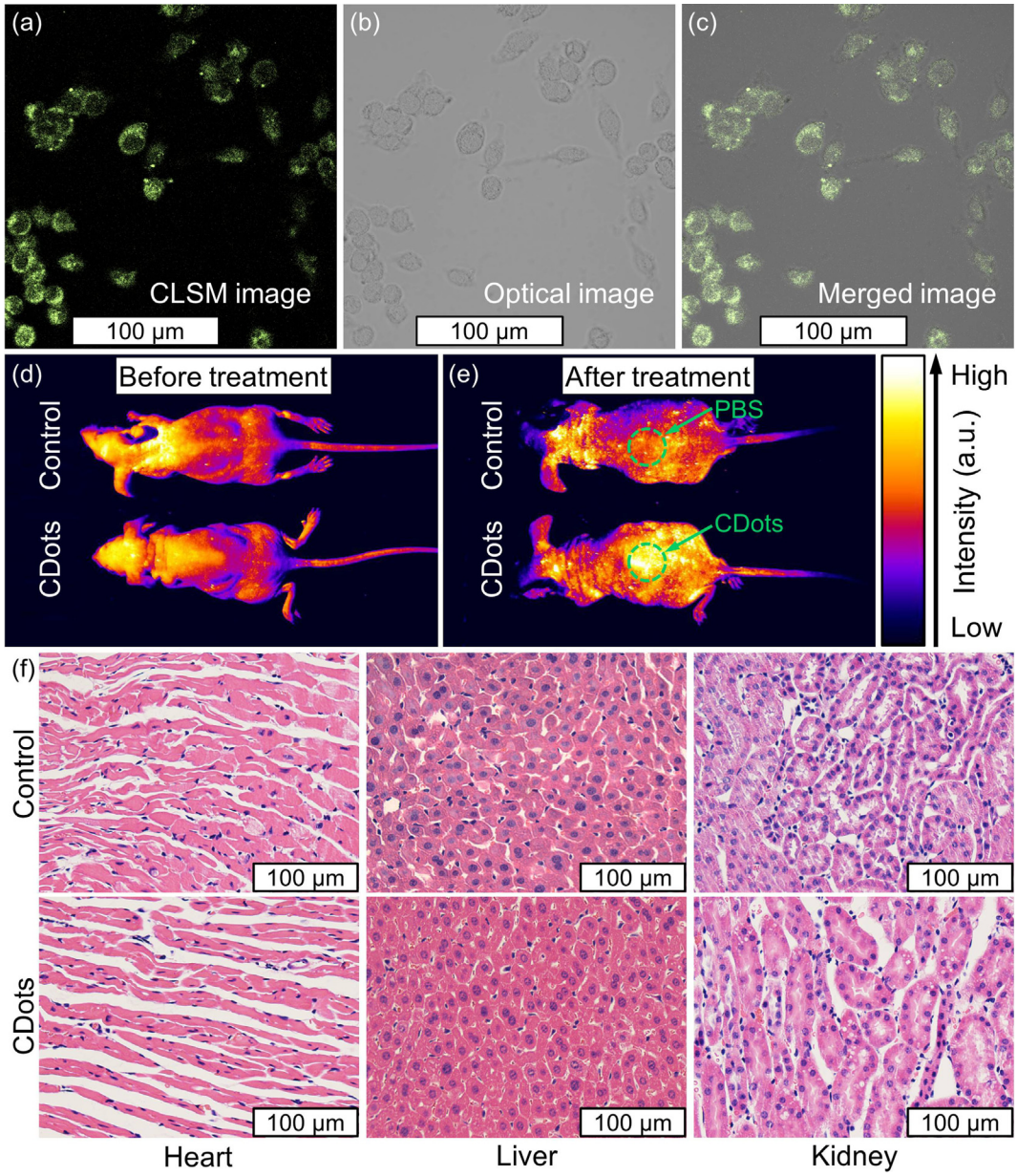

Fig. 5. *In vitro* and *in vivo* fluorescence imaging and corresponding histological evaluation. (a-c) *In vitro* fluorescence cell imaging of CDots-treated RAW264.7 cells: (a) CLSM image, (b) optical image, and (c) merged image of optical and CLSM images. In vivo fluorescence bioimaging in nude mice (d) before and (e) after treatment with PBS or CDots. (f) Histological evaluation of the control and CDots groups. Heart, liver and kidney were harvested after injection of PBS or CDots.

not affect the process. Furthermore, the application of the CDots in *in vivo* fluorescence bioimaging is explored. As shown in Fig. 5d, before the treatment, there are nearly no differences in the fluorescence distribution between the nude mice. After subcutaneously injecting PBS (as a control) or CDots into the nude mice, a photograph of these two mice placed side by side is taken with a 450 nm filter (long pass) under UV light (Fig. 5e). It can be found that the CDots-treated mouse presents a strong PL emission on the back of the mouse in comparison with that of the PBS-treated one. Additionally, hematoxylin and eosin (H&E) staining is performed to evaluate the toxicity of the CDots *in vivo*. Compared with the control group, the images of H&E staining demonstrate that no histological abnormity or pathological changes are found in the important organs of the CDots group, including heart, liver and kidney (Fig. 5f). Our data suggest that the synthesized CDots can be applied as a biological imaging reagent *in vitro* and *in vivo* and possess excellent biocompatibility without side effects.

Besides as the bioimaging reagent, the CDots can also be used as the color conversion layer to design WLEDs. Because the CDots without aggregation-induced fluorescence quenching possess a strong solid-state greenish-yellow fluorescence and a high resistance to organic solvent, the CDots powders can be directly mixed with epoxy-silicon resin, and then the mixture is applied to cover on the blue-emitting chip (405 nm emission) as a conversion layer (Fig. 6a, 6c and S11). After being solidified in an oven at 80 ° C for 1 h, the WLEDs are fabricated. By adjusting the ratios of CDots in the mixture, WLEDs with different color temperatures can be obtained. When the mass ratio of the CDots and epoxy-silicon resin is 1:3, a WLED prototype with CIE coordinates of (0.31, 0.33) and a color temperature of 6646 K is achieved (Fig. 6a and b). By increasing the CDots amount to 1:1, a warm WLED can be built, and its CIE coordinates and color temperature are (0.41, 0.44) and 3735 K, respectively (Fig. 6c and d). Furthermore, owing to the prominent photostability of the CDots (Fig. S4b), the resultant WLEDs present

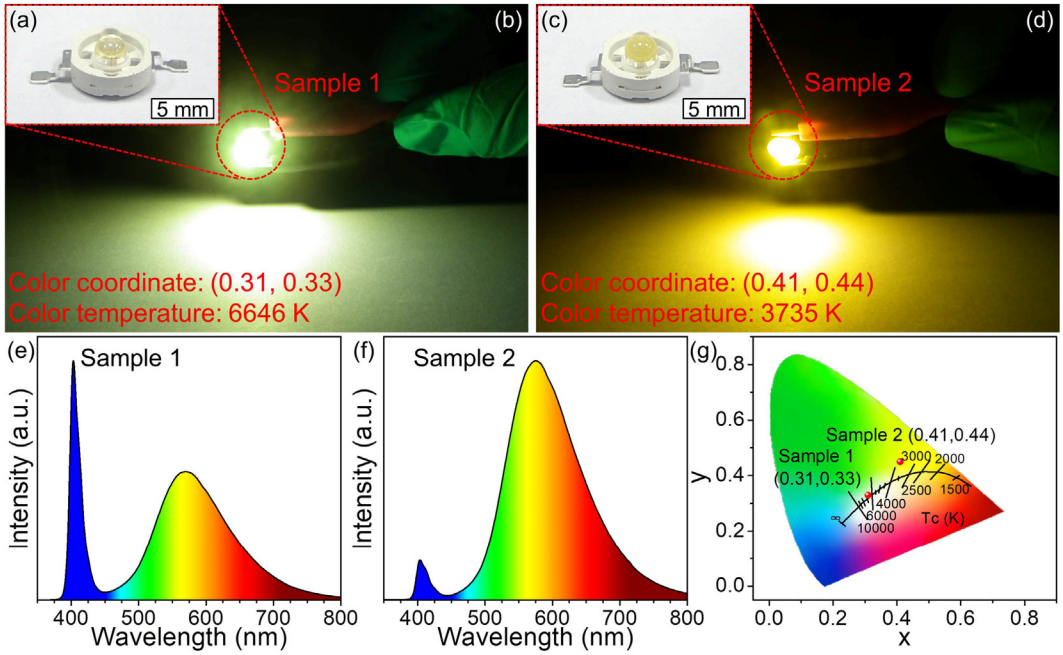

Fig. 6. Fabrication of CDots-based WLEDs. Photographs of the WLEDs prototypes with different CIE coordinates and color temperatures are taken (a and c) under sunlight and (b and d) at work, where the mass ratios of CDots to epoxy-silicon resin are 1:3 in Sample 1 and 1:1 in Sample 2, respectively. (e and f) The corresponding emission spectra of the two WLEDs shown in (b and d). (g) Chromaticity diagram showing the CIE color coordinates of the two WLEDs. The black curve represents the variation of the color temperatures in relation to the CIE color coordinates. The points on the black straight line stand for the constant color temperatures.

good stability (Fig. S12). After continuously working for three weeks, the emission intensity of the WLEDs is nearly unchanged. All these results strongly demonstrate the great potential of our CDots in high performance WLEDs-based illumination applications.

4. Conclusions

Based on the previous researches, realizing the strong fluorescence of CDots in both dispersed and aggregated states is highly desired for promoting the development of CDots-based multiple applications [42,45,50]. In this work, the strong luminescent CDots with a greenish-yellow PL emission in both dispersed and aggregated states are prepared by microwave-assisted heating the mixture of salicylic acid and thiourea in one pot reaction. The doped S element is of great significance in controlling the PL properties of the CDots according to the results of the control test and theoretical calculations, where the doping of S can decrease the bandgap energy, improve the PL intensity, and deteriorate the energy transfer among CDots in aggregates. The resulting CDots are proved to possess nanometer size, excellent biocompatibility, good photostability, strong solid-state fluorescence, as well as remarkable resistance to organic solvent. All these advantages permit CDots to be directly used in multiple applications simultaneously, including *in vitro* and *in vivo* bioimaging and the color conversion layer for WLEDs with different color temperatures [18,44]. We believe that the CDots without the aggregation-induced luminescence quenching will be of great value in developing novel nanoparticles-based luminescent materials and be used in a wider variety of applications therewith.

CRediT authorship contribution statement

Xianjing Li: Methodology, Investigation, Writing – original draft. **Mengdan Zheng:** Methodology, Investigation, Writing – original draft. **Haijing Wang:** Methodology, Data curation, Software. **Yuan Meng:** Formal analysis, Software. **Duan Wang:** Data curation, Software. **Lili Liu:** Software, Visualization. **Qinghui Zeng:** Data curation, Software. **Xiaowei Xu:** Resources, Funding acquisition, Project administration, Validation, Conceptualization, Writing – review & editing. **Ding Zhou:** Resources, Funding acquisition, Project administration, Validation, Conceptualization, Writing – review & editing. **Hongchen Sun:** Resources, Funding acquisition, Project administration, Conceptualization, Supervision, Writing – review & editing.

Declaration of Competing Interest

The authors declare that they have no known competing financial interests or personal relationships that could have appeared to influence the work reported in this paper.

Acknowledgements

This work was supported by grants from the National Key Research and Development Program of China 2016YFC1102800, the National Natural Science Foundation of China (81920108012, 81870741, 81970946 and 62075215), China Postdoctoral Science Foundation (2018 T110259 and 2016 M601386), Jilin Province Science and Technology Research (20180201057YY, 20190103088JH and 20200201611J), Jilin Province Finance Department Science and Technology Research (JCSZ2019378-30), Jilin Province Health Department Youth Science and Technology Research (2019Q014), State Key Laboratory of Luminescence and Applications (SKLA-2020-07), Bai Qiuen Project (2020B43), Open Project of State Key Laboratory of Supramolecular Structure and Materials (sklssm2021038), and JLU Science and Technology Innovative Research Team (2017TD-11).

Appendix A. Supplementary material

Supplementary data to this article can be found online at https://doi.org/10.1016/j.jcis.2021.11.179.

References

[1] X.Q. Xu, H.J. An, D.L. Zhang, H. Tao, Y. Dou, X.H. Li, J. Huang, J.X. Zhang, A self-illuminating nanoparticle for inflammation imaging and cancer therapy, Sci. Adv. 5 (2019) eaat2953.

[2] N.Q. Gong, X.W. Ma, X.X. Ye, Q.F. Zhou, X.A. Chen, X.L. Tan, S.K. Yao, S.D. Huo, T. B. Zhang, S.Z. Chen, X.C. Teng, X.X. Hu, J. Yu, Y.L. Gan, H.D. Jiang, J.H. Li, X.J. Liang, Carbon-dot-supported atomically dispersed gold as a mitochondrial oxidative stress amplifier for cancer treatment, Nat. Nanotechnol. 14 (2019) 379–387.

[3] F.L. Yuan, Y.K. Wang, G. Sharma, Y.T. Dong, X.P. Zheng, P.C. Li, A. Johnston, G. Bappi, J.Z. Fan, H. Kung, B. Chen, M.I. Saidaminov, K. Singh, O. Voznyy, O.M. Bakr, Z.H. Lu, E.H. Sargent, Bright high-colour-purity deep-blue carbon dot light-emitting diodes via efficient edge amination, Nat. Photonics 14 (2019) 171–176.

[4] P. Fan, X. Zhang, H. Deng, X. Guan, Enhanced reduction of *p*-nitrophenol by zerovalent iron modified with carbon quantum dots, Appl. Catal., B 285 (2021) 119829.

[5] Q.Q. Dai, C.E. Duty, M.Z. Hu, Semiconductor-nanocrystals-based white light-emitting diodes, Small 6 (2010) 1577–1588.

[6] E. Jang, S. Jun, H. Jang, J. Lim, B. Kim, Y. Kim, White-light-emitting diodes with quantum dot color converters for display backlights, Adv. Mater. 22 (2010) 3076–3080.

[7] S.H. Li, W. Su, H. Wu, T. Yuan, C. Yuan, J. Liu, G. Deng, X.C. Gao, Z.M. Chen, Y.M. Bao, F.L. Yuan, S.X. Zhou, H.W. Tan, Y.C. Li, X.H. Li, L.Z. Fan, J. Zhu, A.T. Chen, F.Y. Liu, Y. Zhou, M. Li, X.C. Zhai, J.B. Zhou, Targeted tumour theranostics in mice via carbon quantum dots structurally mimicking large amino acids, Nat. Biomed. Eng. 4 (2020) 704–716.

[8] H.Y. Yang, Y.L. Liu, Z.Y. Guo, B.F. Lei, J.L. Zhuang, X.J. Zhang, Z.M. Liu, C.F. Hu, Hydrophobic carbon dots with blue dispersed emission and red aggregation-induced emission, Nat. Commun. 10 (2019) 1789.

[9] C. Zhu, Y. Fu, C. Liu, Y. Liu, L. Hu, J. Liu, I. Bello, H. Li, N. Liu, S. Guo, H. Huang, Y. Lifshitz, S.-T. Lee, Z. Kang, Carbon dots as fillers inducing healing/self-healing and anticorrosion properties in polymers, Adv. Mater. 29 (32) (2017) 1701399.

[10] Q. Jia, J. Ge, W. Liu, X. Zheng, S. Chen, Y. Wen, H. Zhang, P. Wang, A magnetofluorescent carbon dot assembly as an acidic h_2o_2 -driven oxygenerator to regulate tumor hypoxia for simultaneous bimodal imaging and enhanced photodynamic therapy, Adv. Mater. 30 (13) (2018) 1706090.

[11] B.W. Yao, H. Huang, Y. Liu, Z.H. Kang, Carbon dots: A small conundrum, Trends Chem. 1 (2019) 235–246.

[12] Z. Zhu, R. Cheng, L. Ling, Q. Li, S.u. Chen, Rapid and large-scale production of multi-fluorescence carbon dots by a magnetic hyperthermia method, Angew. Chem., Int. Ed. 59 (8) (2020) 3099–3105.

[13] A. Xu, G. Wang, Y. Li, H. Dong, S. Yang, P. He, G. Ding, Carbon-based quantum dots with solid-state photoluminescent: mechanism, implementation, and application, Small 16 (48) (2020) 2004621.

[14] F. Li, S. Li, X.C. Guo, Y.H. Dong, C. Yao, Y.P. Liu, Y.G. Song, X.L. Tan, L.Z. Gao, D.Y. Yang, Chiral carbon dots mimicking topoisomerase i to mediate the topological rearrangement of supercoiled DNA enantioselectively, Angew. Chem., Int. Ed. 59 (2020) 11087–11092.

[15] M. Park, H.S. Kim, H. Yoon, J. Kim, S. Lee, S. Yoo, S. Jeon, Controllable singlet-triplet energy splitting of graphene quantum dots through oxidation: from phosphorescence to tadf, Adv. Mater. 32 (31) (2020) 2000936.

[16] C.H. Yang, H. Aslan, P. Zhang, S.J. Zhu, Y. Xiao, L.X. Chen, N. Khan, T. Boesen, Y.L. Wang, Y. Liu, L. Wang, Y. Sun, Y.J. Feng, F. Besenbacher, F. Zhao, M. Yu, Carbon dots-fed *shewanella oneidensis* mr-1 for bioelectricity enhancement, Nat. Commun. 11 (2020) 1379.

[17] N.V. Tepliakov, E.V. Kundelev, P.D. Khavlyuk, Y. Xiong, M.Y. Leonov, W.R. Zhu, A.V. Baranov, A.V. Fedorov, A.L. Rogach, I.D. Rukhlenko, Sp^2-sp^3-hybridized atomic domains determine optical features of carbon dots, ACS Nano 13 (2019) 10737–10744.

[18] H.J. Liu, X.T. Lv, J.C. Qian, H. Li, Y. Qian, X.Y. Wang, X.F. Meng, W.C. Lin, H. Wang, Graphitic carbon nitride quantum dots embedded in carbon nanosheets for near-infrared imaging-guided combined photo-chemotherapy, ACS Nano 14 (2020) 13304–13315.

[19] B. Li, S. Zhao, L.i. Huang, Q. Wang, J. Xiao, M. Lan, Recent advances and prospects of carbon dots in phototherapy, Chem. Eng. J. 408 (2021) 127245.

[20] Y.L. Xu, Y. Yang, S. Lin, L.H. Xiao, Red-emitting carbon nanodot-based wide-range responsive nanothermometer for intracellular temperature sensing, Anal. Chem. 92 (2020) 15632–15638.

[21] S. Tao, S. Lu, Y. Geng, S. Zhu, S.A.T. Redfern, Y. Song, T. Feng, W. Xu, B. Yang, Design of metal-free polymer carbon dots: a new class of room-temperature phosphorescent materials, Angew. Chem., Int. Ed. 57 (9) (2018) 2393–2398.

[22] N. Soni, S. Singh, S. Sharma, G. Batra, K. Kaushik, C. Rao, N.C. Verma, B. Mondal, A. Yadav, C.K. Nandi, Absorption and emission of light in red emissive carbon nanodots, Chem. Sci. 12 (2021) 3615–3626.

[23] Y. Yan, J. Gong, J. Chen, Z. Zeng, W. Huang, K. Pu, J. Liu, P. Chen, Recent advances on graphene quantum dots: from chemistry and physics to applications, Adv. Mater. 31 (21) (2019) 1808283.

[24] U. Lee, E. Heo, T.-H. Le, H. Lee, S. Kim, S. Lee, H. Jo, H. Yoon, Carbon dots for epoxy curing: anti-forgery patterns with long-term luminescent stability, Chem. Eng. J. 405 (2021) 126988.

[25] S. Sun, Q. Chen, Z. Tang, C. Liu, Z. Li, A. Wu, H. Lin, Tumor microenvironment stimuli-responsive fluorescence imaging and synergistic cancer therapy by carbon-dot-cu^{2+} nanoassemblies, Angew. Chem., Int. Ed. 59 (47) (2020) 21041–21048.

[26] Y.Q. Sun, S.T. Liu, L.Y. Sun, S.S. Wu, G.Q. Hu, X.L. Pang, A.T. Smith, C.F. Hu, S.S. Zeng, W.X. Wang, Y.L. Liu, M.T. Zheng, Ultralong lifetime and efficient room temperature phosphorescent carbon dots through multi-confinement structure design, Nat. Commun. 11 (2020) 5591.

[27] Q. Wang, J. Li, X.J. Tu, H.B. Liu, M. Shu, R. Si, C.T.J. Ferguson, K.A.I. Zhang, R. Li, Single atomically anchored cobalt on carbon quantum dots as efficient photocatalysts for visible light-promoted oxidation reactions, Chem. Mater. 32 (2019) 734–743.

[28] M. Cacioppo, T. Scharl, L. Đorđević, A. Cadranel, F. Arcudi, D.M. Guldi, M. Prato, Symmetry-breaking charge-transfer chromophore interactions supported by carbon nanodots, Angew. Chem., Int. Ed. 59 (31) (2020) 12779–12784.

[29] W.W. Chen, Z.J. Qin, B. McElhenny, F.H. Zhang, S. Chen, J. Bao, Z.M. Wang, H.Z. Song, Z.F. Ren, The effect of carbon quantum dots on the electrocatalytic hydrogen evolution reaction of manganese–nickel phosphide nanosheets, J. Mater. Chem. A 7 (2019) 21488–21495.

[30] H. Jia, Z. Wang, T. Yuan, F. Yuan, X. Li, Y. Li, Z. Tan, L. Fan, S. Yang, Electroluminescent warm white light-emitting diodes based on passivation enabled bright red bandgap emission carbon quantum dots, Adv. Sci. 6 (13) (2019) 1900397.

[31] J. Li, S. Yang, Y. Deng, P. Chai, Y. Yang, X. He, X. Xie, Z. Kang, G. Ding, H. Zhou, X. Fan, Emancipating target-functionalized carbon dots from autophagy vesicles for a novel visualized tumor therapy, Adv. Funct. Mater. 28 (30) (2018) 1800881.

[32] F. Ostadhossein, L. Benig, I. Tripathi, S.K. Misra, D. Pan, Fluorescence detection of bone microcracks using monophosphonated carbon dots, ACS Appl. Mater. Interfaces 10 (2018) 19408–19415.

[33] D.K. Khajuria, V.B. Kumar, D. Gigi, A. Gedanken, D. Karasik, Accelerated bone regeneration by nitrogen-doped carbon dots functionalized with hydroxyapatite nanoparticles, ACS Appl. Mater. Interfaces 10 (2018) 19373–19385.

[34] X. Yang, L. Sui, B. Wang, Y. Zhang, Z. Tang, B. Yang, S. Lu, Red-emitting, self-oxidizing carbon dots for the preparation of white LEDs with super-high color rendering index, Sci. China: Chem. 64 (2021) 1547–1553.

[35] S. Lu, L. Sui, J. Liu, S. Zhu, A. Chen, M. Jin, B. Yang, Near-infrared photoluminescent polymer-carbon nanodots with two-photon fluorescence, Adv. Mater. 29 (15) (2017) 1603443.

[36] S. Liu, X. Yi, X. Wu, Q. Li, Y. Wang, Internalized carbon dots for enhanced extracellular electron transfer in the dark and light, Small 16 (44) (2020) 2004194.

[37] Y.J. Chung, C.H. Lee, J. Lim, J. Jang, H. Kang, C.B. Park, Photomodulating carbon dots for spatiotemporal suppression of alzheimer's β-amyloid aggregation, ACS Nano 14 (2020) 16973–16983.

[38] Y.C. Wang, U. Kadiyala, Z.B. Qu, P. Elvati, C. Altheim, N.A. Kotov, A. Violi, J.S. VanEpps, Anti-biofilm activity of graphene quantum dots *via* self-assembly with bacterial amyloid proteins, ACS Nano 13 (2019) 4278–4289.

[39] X. Zhang, H. Yang, Z. Wan, T. Su, X. Zhang, J. Zhuang, B. Lei, Y. Liu, C. Hu, Self-quenching-resistant red emissive carbon dots with high stability for warm white light-emitting diodes with a high color rendering index, Adv. Opt. Mater. 8 (15) (2020) 2000251.

[40] L. Wang, W.T. Li, L.Q. Yin, Y.J. Liu, H.Z. Guo, J.W. Lai, Y. Han, G. Li, M. Li, J.H. Zhang, R. Vajtai, P.M. Ajayan, M.H. Wu, Full-color fluorescent carbon quantum dots, Sci. Adv. 6 (2020) eabb6772.

[41] X. Miao, D. Qu, D. Yang, B. Nie, Y. Zhao, H. Fan, Z. Sun, Synthesis of carbon dots with multiple color emission by controlled graphitization and surface functionalization, Adv. Mater. 30 (1) (2018) 1704740.

[42] H. Ding, J.-S. Wei, P. Zhang, Z.-Y. Zhou, Q.-Y. Gao, H.-M. Xiong, Solvent-controlled synthesis of highly luminescent carbon dots with a wide color gamut and narrowed emission peak widths, Small 14 (22) (2018) 1800612.

[43] J.B. Essner, J.A. Kist, L. Polo-Parada, G.A. Baker, Artifacts and errors associated with the ubiquitous presence of fluorescent impurities in carbon nanodots, Chem. Mater. 30 (2018) 1878–1887.

[44] T. Meng, Z. Wang, T. Yuan, X. Li, Y. Li, Y. Zhang, L. Fan, Gram-scale synthesis of highly efficient rare-earth element-free red/green/blue solid-state bandgap fluorescent carbon quantum rings for white light-emitting diodes, Angew. Chem., Int. Ed. 60 (30) (2021) 16343–16348.

[45] M. Park, Y. Jeong, H.S. Kim, W. Lee, S.-H. Nam, S. Lee, H. Yoon, J. Kim, S. Yoo, S. Jeon, Quenching-resistant solid-state photoluminescence of graphene quantum dots: Reduction of $\pi-\pi$ stacking by surface functionalization with poss, peg, and hda, Adv. Funct. Mater. 31 (29) (2021) 2102741.

[46] J. Yang, H. Miao, J. Jing, Y. Zhu, W. Choi, Photocatalytic activity enhancement of pdi supermolecular via π-π action and energy level adjusting with graphene quantum dots, Appl. Catal., B 281 (2021) 119547.

[47] Y.-C. Liang, S.-S. Gou, K.-K. Liu, W.-J. Wu, C.-Z. Guo, S.-Y. Lu, J.-H. Zang, X.-Y. Wu, Q. Lou, L. Dong, Y.-F. Gao, C.-X. Shan, Ultralong and efficient phosphorescence from silica confined carbon nanodots in aqueous solution, Nano Today 34 (2020) 100900.

[48] C.L. Shen, J.H. Zang, Q. Lou, L.X. Su, Z. Li, Z.Y. Liu, L. Dong, C.X. Shan, In-situ embedding of carbon dots in a trisodium citrate crystal matrix for tunable solid-state fluorescence, Carbon 136 (2018) 359–368.

[49] J. Liu, N. Wang, Y. Yu, Y. Yan, H. Zhang, J. Li, J. Yu, Carbon dots in zeolites: A new class of thermally activated delayed fluorescence materials with ultralong lifetimes, Sci. Adv. 3 (5) (2017).
[50] J.L. Wang, Q. Li, J.X. Zheng, Y.Z. Yang, X.G. Liu, B.S. Xu, N, b-codoping induces high-efficiency solid-state fluorescence and dual emission of yellow/orange carbon dots, ACS Sustain. Chem. Eng. 9 (2021) 2224–2236.
[51] P. Garg, S. Sangam, D. Kochhar, S. Pahari, C. Kar, M. Mukherjee, Exploring the role of triazole functionalized heteroatom co-doped carbon quantum dots against human coronaviruses, Nano Today 35 (2020) 101001.
[52] G. Murali, J.K.R. Modigunta, S. Park, S. Lee, H. Lee, J. Yeon, H. Kim, Y.H. Park, S.Y. Park, J.R. Durrant, H. Cha, T.K. An, I. In, Enhancing light absorption and prolonging charge separation in carbon quantum dots via cl-doping for visible-light-driven photocharge-transfer reactions, ACS Appl. Mater. Interfaces 13 (2021) 34648–34657.
[53] J.K. Yu, X. Yong, Z.Y. Tang, B. Yang, S.Y. Lu, Theoretical understanding of structure-property relationships in luminescence of carbon dots, J Phys. Chem. Lett. 12 (2021) 7671–7687.
[54] Z.Q. Zhu, X.H. Li, M. Luo, M.Z. Chen, W.M. Chen, P. Yang, X.Y. Zhou, Synthesis of carbon dots with high photocatalytic reactivity by tailoring heteroatom doping, J. Colloid Interface Sci. 605 (2021) 330–341.
[55] Y. Li, X. Xu, B. Lei, J. Zhuang, X. Zhang, C. Hu, J. Cui, Y. Liu, Magnesium-nitrogen co-doped carbon dots enhance plant growth through multifunctional regulation in photosynthesis, Chem. Eng. J. 422 (2021) 130114.
[56] M. Zhang, X. Zhai, T. Ma, Y. Huang, C. Yan, Y. Du, Multifunctional cerium doped carbon dots nanoplatform and its applications for wound healing, Chem. Eng. J. 423 (2021) 130301.
[57] L. Ai, Y. Yang, B. Wang, J. Chang, Z. Tang, B. Yang, S. Lu, Insights into photoluminescence mechanisms of carbon dots: advances and perspectives, Sci. Bull. 66 (2021) 839–856.
[58] S.N. Qu, X.Y. Liu, X.Y. Guo, M.H. Chu, L.G. Zhang, D.Z. Shen, Amplified spontaneous green emission and lasing emission from carbon nanoparticles, Adv. Funct. Mater. 24 (2014) 2689–2695.
[59] C. Feng, L. Tang, Y. Deng, J. Wang, Y. Liu, X. Ouyang, H. Yang, J. Yu, J. Wang, A novel sulfur-assisted annealing method of g-c_3n_4 nanosheet compensates for the loss of light absorption with further promoted charge transfer for photocatalytic production of h_2 and h_2o_2, Appl. Catal., B 281 (2021) 119539.
[60] S. Franke, J. Ren, M. Richter, A. Knorr, S. Hughes, Fermi's golden rule for spontaneous emission in absorptive and amplifying media, Phys. Rev. Lett. 127 (1) (2021) 013602.